AAE 59000 ACA Final Project Report
Optimal Control and Momentum Exchange Tethers

Andrew Binder, Abdulrahman Abdrabou

Due: April 28, 2024

1 Introduction and Problem Statement

Momentum exchange tethers present a new and numerous challenges in the astrodynamics field. The use of these tethers can provide a promising solution to for spacecraft propulsion and trajectory optimization. More specifically, there has been an increased interest for exploration in the cislunar region as scientific and commerical missions have been rapidly expanding. Achieving optimal control solutions in such region with more complex environment and dynamics is a challenging problem but necessary for the design and operation of missions.

Thus, this study aims to investigate the integration of optimal control and momentum exchange tethers in the cislunar region. By developing advanced control algorithms and optimization techniques to guide payloads into catch opportunities with the tether, the objective is to maximize the efficiency, reliability, and versatility of spacecraft operations in this dynamic and challenging environment. Through comprehensive simulations and analyses, this research seeks to provide valuable insights and guidelines for the design and implementation of future cislunar missions and space infrastructure.

A study conducted by Kayama et al. in 2022 [3], explored the use of successive convex optimization techniques for designing low-thrust trajectories in the Circular Restricted Three-Body Problem (CR3BP) environment. The dynamics near Lagrange points and the Moon are highly nonlinear, making the solution more intricate and requiring more repeated attempts (convexifications) at solving the problem. The researchers propagated the solutions to obtain a transfer from a Halo orbit to a Near Rectlinear Halo Orbit (NRHO), aiming to achieve an optimal trajectory approximating the solution within the CR3BP framework.

The rest of the paper will provide a detailed explanation of: the problem setup, derivation of dynamics and optimal control conditions, simulation results, and finally conclusion.

2 Objectives

Our objectives were classified into three main levels. These levels were defined in a way that makes it easy to follow and understand, and makes a smooth transition in complexity levels using content from class.

Our objectives list can be summarized below. These are goals we will work towards achieving.

1. Level 1: Acquire a variety of catch opportunities using a minimum energy formulation
2. Level 2: Achieve a minimum energy $\rightarrow$ minimum fuel homotopy between the two transfer objectives.
3. Level 3: Add control of the tether's rotation rate to the scheme, ideally reducing fuel costs required of the payload.

This list contains tasks that demonstrate basic understanding of the material/-content and the problem such as Level 1. It also contains objectives that pose more challenge.

2.1 Level 1

This goal is made to provide a basic understanding of the problem which includes defining the minimum energy cost function and the governing dynamical model of the payload and the tether. Using this setup, a slew of optimal trajectories could be acquired, parameterizing what these catches look like over time. An important task is deriving the equations of motion of the rendezvous target, the tether tip, because its dynmaical model is essential to our problem.

2.2 Level 2

With Level 1 completed, we can now focus on modifying the simulation to account for minimum fuel instead. By solving the minimum energy problem first, using Pontryagin's Minimum principle and numerical homotopy techniques, these minimum energy trajectories could be continuously deformed into minimum fuel ones. Other optimization problems may still be explored at this level of the project.

2.3 Level 3

Level 3 is our most challenging and ambitious objective. Simulating a system with variable tether speed can change the results of the optimization problems significantly. Assuming that spin control is a factor, theoretically fuel costs could be lowered (even considerably). Introducing such a change would provide valuable insights into the momentum exchange tether feasibility in cislunar space.

Group Contribution All group members contributed equally to the project. All tasks were accomplished together and had equal contributions from the entire team.

3 Methods

3.1 Level 1: Derivation of minimum-energy controlled dynamics

In order to properly formulate the optimization problem, we need to define the dynamics that the spacecraft is under in the region. The CR3BP is governed by the following dynamics:

$$\begin{aligned}
\ddot{x} &= 2\dot{y} + x - \frac{(1-\mu)(x+\mu)}{d^3} - \frac{\mu(x-1+\mu)}{r^3} \\
\ddot{y} &= -2\dot{x} + y - \frac{(1-\mu)y}{d^3} - \frac{\mu\, y}{r^3} \\
\ddot{z} &= -\frac{(1-\mu)z}{d^3} - \frac{\mu\, z}{r^3}
\end{aligned} \tag{1}$$

Thrusters produce inertial forces compatible with Newton's Second Law. Without a loss in generality, we can presume that thrusts are performed within the synodic corotating frame of the Earth and the Moon. We can express the controlled equations of motion as:

$$\dot{\mathbf{x}} = \mathbf{f}_0(\mathbf{x}, t) + B\mathbf{u} \tag{2}$$

Where $\mathbf{f}_0$ is our original dynamics:

$$\mathbf{f}_0(\mathbf{x}, t) = \begin{bmatrix} \dot{\mathbf{x}} \\ \dot{\mathbf{y}} \\ \dot{\mathbf{z}} \\ f_x \\ f_y \\ f_z \end{bmatrix} = \begin{bmatrix} \dot{\mathbf{x}} \\ \dot{\mathbf{y}} \\ \dot{\mathbf{z}} \\ 2\dot{y} + x - \frac{(1-\mu)(x+\mu)}{d^3} - \frac{\mu(x-1+\mu)}{r^3} \\ -2\dot{x} + y - \frac{(1-\mu)y}{d^3} - \frac{\mu\, y}{r^3} \\ -\frac{(1-\mu)z}{d^3} - \frac{\mu\, z}{r^3} \end{bmatrix} \tag{3}$$

and where B is the autonomous matrix:

$$B = \begin{bmatrix} 0 & 0 & 0 \\ 0 & 0 & 0 \\ 0 & 0 & 0 \\ 1 & 0 & 0 \\ 0 & 1 & 0 \\ 0 & 0 & 1 \end{bmatrix} \tag{4}$$

We can note (for ease of derivations later) that the equations of motion can be derived from a pseudopotential function $U(\rho)$:

$$U(\rho) = \frac{1}{2}(x^2 + y^2) + \frac{1-\mu}{d} + \frac{\mu}{r} \tag{5}$$

We can rewrite the differential equations that govern the spacecraft's motion in the nondimensionalized synodic frame as a function of the gradient of this pseudopotential:

$$\begin{aligned} \ddot{x} - 2\dot{y} &= \frac{\partial U}{\partial x} \\ \ddot{y} + 2\dot{x} &= \frac{\partial U}{\partial y} \\ \ddot{z} &= \frac{\partial U}{\partial z} \end{aligned} \tag{6}$$

This means that we can define our original dynamics $\mathbf{f}_0$ quite succinctly:

$$\mathbf{f}_0(\mathbf{x}, t) = \begin{bmatrix} \dot{\mathbf{x}} \\ \dot{\mathbf{y}} \\ \dot{\mathbf{z}} \\ f_x \\ f_y \\ f_z \end{bmatrix} = \begin{bmatrix} \dot{\mathbf{x}} \\ \dot{\mathbf{y}} \\ \dot{\mathbf{z}} \\ 2\dot{y} + \partial U/\partial x \\ -2\dot{x} + \partial U/\partial y \\ \partial U/\partial z \end{bmatrix} \tag{7}$$

For ease of notation, let the vector $\mathbf{g} = \begin{bmatrix} f_x, & f_y, & f_z \end{bmatrix}^T$.

The motion of the rendezvous target, i.e. the tether's tip: The tether currently sits in an L_1 halo orbit. It is straightforward to decompose the motion of the tip of the tether as the motion of the tether's center of mass in it's orbit, plus the rotation of the tether. Presumably, initial conditions and a state history for the Halo orbit can be solved for a priori. The time histories of the position of velocity can be represented by this Halo orbit periodic solution $\mathbf{h}_{\text{halo}}(t) = \begin{bmatrix} \mathbf{r}_{\text{halo}}^T, & \mathbf{v}_{\text{halo}}^T \end{bmatrix}^T$. The remaining quantity is the motion of the tether's tip. Approximating the tether as a rigid body, the tether rotates at a constant rate in the inertial frame. For the sake of this analysis, we presume that the tether rotates only in the plane of the Earth and the Moon's rotation. The tether's tip under the mentioned assumptions, stays at a constant distance from the tether's center of mass, and at a direction fixed in the tether's body frame $\mathcal{B}$. The position of the tip in this frame is $\mathbf{h}_{\text{tip}} = L \cdot \hat{\mathbf{b}}_1$ From an inertial perspective, this means that the tether's rotation proceeds at a constant rate $\dot{\alpha}$. The motion of the tether's tip in the inertial frame then is described by applying

the following rotation:

$$\mathbf{h}_{\text{tip}} = \begin{bmatrix} \cos\alpha & \sin\alpha & 0 \\ -\sin\alpha & \cos\alpha & 0 \\ 0 & 0 & 1 \end{bmatrix} \begin{bmatrix} L \\ 0 \\ 0 \end{bmatrix} = L\cos\alpha \cdot \hat{\mathbf{X}} + L\sin\alpha \cdot \hat{\mathbf{Y}} \tag{8}$$

$\alpha = \dot{\alpha}(t - t_0)$, where t is the current time and t_0 is some epoch time for which the tether is oriented such that it is colinear to the inertial $\hat{\mathbf{X}}$. If $\dot{\alpha}$ is defined positive in the angular momentum direction of the Earth and Moon's orbit, the (nondimensionalized) position of the tether's tip in the Earth-Moon synodic frame can be written as follows:

$$\mathbf{h}_{\text{tip}} = \mathbf{r}_{\text{halo}} + \begin{bmatrix} \frac{L}{l^*}\cos\left[(\frac{\dot{\alpha}}{n} - 1)(\tau - \tau_0)\right] \\ \frac{L}{l^*}\sin\left[(\frac{\dot{\alpha}}{n} - 1)(\tau - \tau_0)\right] \\ 0 \end{bmatrix} \tag{9}$$

This equation intuitively makes sense. When $\dot{\alpha} = n$, the tether's tip rotates at the same rate as the Earth-Moon corotating frame. The tip then will be oriented at a constant direction and distance in the synodic frame, moving at the same velocity as the tether's center of mass. For simplicity's sake, we will give names to all of these nondimensional parameters. If we make the substitutions that $\tilde{l} = L/l^*$ (constant) and $\tilde{\alpha} = \alpha/n - 1$ (constant), we can write the tip's position more simply:

$$\mathbf{h}_{\text{tip}} = \mathbf{r}_{\text{halo}} + \tilde{l}\begin{bmatrix} \cos\left[\tilde{\alpha}(\tau - \tau_0)\right] \\ \sin\left[\tilde{\alpha}(\tau - \tau_0)\right] \\ 0 \end{bmatrix} \tag{10}$$

For later, we are also interested in the rotating frame velocity and acceleration of the tether's tip. To get these vectors, we can perform derivatives $\frac{\partial}{\partial\tau}[\mathbf{h}_{\text{tip}}]$. For synodic-frame velocity:

$$\frac{\partial}{\partial\tau}[\mathbf{h}_{\text{tip}}] = \dot{\mathbf{h}}_{\text{tip}} = \frac{\partial}{\partial\tau}\left[\mathbf{r}_{\text{halo}} + \tilde{l}\begin{bmatrix} \cos\left[\tilde{\alpha}(\tau - \tau_0)\right] \\ \sin\left[\tilde{\alpha}(\tau - \tau_0)\right] \\ 0 \end{bmatrix}\right] = \mathbf{v}_{\text{halo}} + \tilde{l}\tilde{\alpha}\begin{bmatrix} -\sin\left[\tilde{\alpha}(\tau - \tau_0)\right] \\ \cos\left[\tilde{\alpha}(\tau - \tau_0)\right] \\ 0 \end{bmatrix} \tag{11}$$

and, by a similar process for the synodic-frame acceleration:

$$\frac{\partial}{\partial\tau}\left[\dot{\mathbf{h}}_{\text{tip}}\right] = \ddot{\mathbf{h}}_{\text{tip}} = \mathbf{a}_{\text{halo}} - \tilde{l}\tilde{\alpha}^2\begin{bmatrix} \cos\left[\tilde{\alpha}(\tau - \tau_0)\right] \\ \sin\left[\tilde{\alpha}(\tau - \tau_0)\right] \\ 0 \end{bmatrix} \tag{12}$$

Fig.1a below shows the configuration of the tether. As illustrated in the figure, the location of the tether is not fixed and changes over time. Fig.1b provides a zoomed-in view, demonstrating the tether's movement. As described mathematically, the tether's center of mass follows an L_1 halo orbit. Within this orbit, the tether rotates about it's center of mass. The thorough understanding of the superposition of this translation and rotation is crucial, as the tether's tip hosts a docking mechanism. Successful rendezvous with the tether's tip is the only mechanism by which a catch can be achieved.

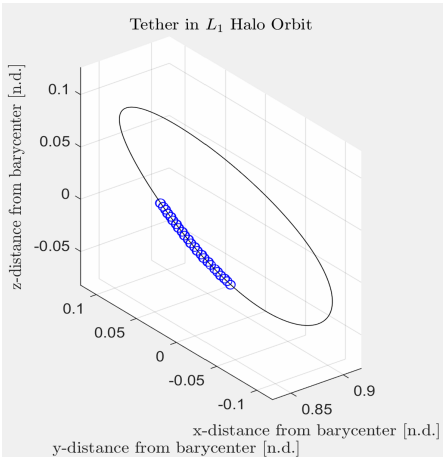

(a) Tether stationed in L_1 Halo Orbit

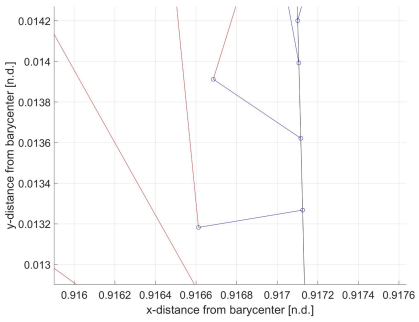

(b) Zoomed in view on tether motion

Figure 1: Tether motion in Halo Orbit

Derivation of optimal control: For our minimum energy problem, we define the cost function, **J** as follows:

$$J = \int_{t_0}^{t_f} ||\mathbf{u}||_2^2 dt \tag{13}$$

The control Lagrangian can be defined as:

$$L = ||\mathbf{u}||_2^2 = \mathbf{u} \cdot \mathbf{u} \tag{14}$$

Combining that with our Lagrange multipliers, we can formulate our control Hamiltonian:

$$H = L + \lambda^T \mathbf{f} = \mathbf{u} \cdot \mathbf{u} + \lambda^T (\mathbf{f}_0 + B\mathbf{u}) = \mathbf{u} \cdot \mathbf{u} + \lambda^T \mathbf{f}_0 + \lambda^T B\mathbf{u} \tag{15}$$

From our control Hamiltonian, we can define our state evolution:

$$\dot{\mathbf{x}} = \mathbf{f}_0 + B\mathbf{u} \tag{16}$$

and our costate evolution:

$$\dot{\lambda}^T = -H_{\mathbf{x}} = -\lambda^T \frac{\partial}{\partial \mathbf{x}} \left[\mathbf{f}_0 + B\mathbf{u}\right] = -\lambda^T \frac{\partial \left[\mathbf{f}_0\right]}{\partial \mathbf{x}} \tag{17}$$

$$\frac{\partial \left[\mathbf{f}_0\right]}{\partial \mathbf{x}} = \begin{bmatrix} \frac{\partial [\mathbf{v}]}{\partial \mathbf{r}} & \frac{\partial [\mathbf{v}]}{\partial \mathbf{v}} \\ \frac{\partial}{\partial \mathbf{r}} [g] & \Omega \end{bmatrix} = \begin{bmatrix} \mathbf{0}_{3\times 3} & \mathbf{I}_{3\times 3} \\ U_{pp} & \Omega \end{bmatrix} \tag{18}$$

Where U_{pp} is the symmetric Hessian matrix of $\mathbf{g}$ with respect to our position vector $\mathbf{p} = \begin{bmatrix} x, & y, & z \end{bmatrix}^T$. The total matrix $\frac{\partial}{\partial \mathbf{x}} [\mathbf{f}_0]$ is well-known in the literature - it is otherwise known as the 'A' matrix, used in the CR3BP to define the time evolution of the state-only transition matrix. Writing this in it's most condensed and untransposed form, the costate's evolution follows the following dynamics:

$$\dot{\lambda} = -A^T \lambda \tag{19}$$

Our optimal control is governed by $H_{\mathbf{u}} = \mathbf{0}$:

$$H_{\mathbf{u}} = \frac{\partial}{\partial \mathbf{u}} \left[\mathbf{u} \cdot \mathbf{u} + \lambda^T \mathbf{f}_0 + \lambda^T B \mathbf{u} \right] = 2\mathbf{u}^T + \lambda^T B = \mathbf{0} \tag{20}$$

Which, when solving for the control:

$$\mathbf{u}^* = -\frac{1}{2} B^T \lambda = \frac{1}{2} \mathbf{p} \tag{21}$$

where $\mathbf{p}$ is the primer vector. While we're here:

$$H_{\mathbf{uu}} = 2I_{2\times 2} \geq 0 \tag{22}$$

To address the remainder of the transversality conditions, it is important to define what can vary and what cannot. Using the formulation in class as our guide, we hold our initial and final positions to be constants and our initial time to be constant. While generally this would lead to the introduction of the transversality condition that $\nu^T \psi_{t_f} + H(t_f) = 0$, for our case we seek to perform a continuation over many final different times. While always possible to include the transversality condition and sweep through final times via a natural parameter continuation, this method may not be the best choice for the analysis we desire to do. If we choose to neglect the transversality condition, our Jacobian $\partial\psi/\partial Z$ becomes nonsquare and for the Newton-Raphson scheme we will use to drive $\psi = \mathbf{0}$, classically uninvertible. This is a nonissue in general, as pseudoinverses exist (like the Moore-Penrose pseudoinverse) that compensate for the matrix's nonsquare nature. Following this line of thought, our residual vector is:

$$\psi = \mathbf{0} \tag{23}$$

Since $d\nu \neq 0$. We seek to target full-state equivalence, so specifically the residual will be driven to:

$$\psi = \left[\mathbf{x}(t_f) - \mathbf{x}_{\mathrm{TT}}(t_f) \right] \tag{24}$$

where $\mathbf{x}_{\mathrm{TT}}(t_f)$ is the location and velocity of the tether's tip at the chosen final time t_f. Our control variables $\mathbf{Z}$ are:

$$\mathbf{Z} = \begin{bmatrix} \lambda_0 \\ t_f \end{bmatrix} \tag{25}$$

Our Jacobian $\partial\psi/\partial Z$ is:

$$\frac{\partial\left[\psi\right]}{\partial Z} = \begin{bmatrix} \frac{\partial[x_f]}{\partial\lambda_0} & \frac{\partial[x_f - \mathbf{x}_{\mathrm{TT}}]}{\partial t_f} \end{bmatrix} \tag{26}$$

The matrix $\partial x_f/\partial\lambda_0$ are elements of the augmented state transition matrix and the vector $\frac{\partial}{\partial t_f}\left[x_f - \mathbf{x}_{\mathrm{TT}}\right]$ is:

$$\frac{\partial\left[x_f - \mathbf{x}_{\mathrm{TT}}\right]}{\partial t_f} = \dot{\mathbf{x}} - \dot{\mathbf{x}}_{\mathrm{TT}} \tag{27}$$

where the column vector $\dot{\mathbf{x}}_{\mathrm{TT}} = \begin{bmatrix} \dot{\mathbf{h}}_{\mathrm{tip}}^T, & \ddot{\mathbf{h}}_{\mathrm{tip}}^T \end{bmatrix}^T$. The equations of motion for the augmented state transition matrix (or, as discussed in Section 6.1, the *state-costate transition matrix*) can be calculated analytically, a derivation which can be found in Section 6.1. This SCTM can be integrated alongside our equations of motion.

For this particular section, convergence onto controlled state histories was done without prebuilt tools like MATLAB's *fsolve* or similar. Instead, we implemented our own. For this problem, our control variables Z are of size 7×1, and our constraint vector ψ is of size 6×1. When taking the Jacobian $\frac{\partial[\psi]}{\partial Z}$, the resultant matrix is consequentially a dense 6×7 and has a nontrivial one-dimensional null-space as a result. Since the tether can, in principle, rotate quickly with respect to the other dynamics, it is understandable that finding initial conditions that rendezvous with the tether's tip could be a quite sensitive process. This sensitivity could be alleviated by using a previously-converged trajectory to feed information forward into the next convergence process. When done intelligently, a guess at the initial condition can be provided that gets quite close to where the eventually-converged IC will be. One way to seed this information is by using a pseudo-arclength continuation (PAC) scheme [2]. An adaptive-stepsize PAC scheme was implemented to seed initial guesses for the convergence process.

3.2 Level 2: Achieve a minimum energy → minimum fuel homotopy between the two transfer objectives

In order to achieve a smooth transition from minimum energy to minimum fuel, a continuation homotopy method is implemented. This problem can be formulated as a blended-objective cost function by including a sliding parameter. By the implicit function theorem, if a solution exists corresponding to one certain value of the sliding parameter and derivatives with respect to the parameter there are well-defined, then within the neighborhood of the blended-objective cost function, the derivatives must also be well-defined. By including the minimum energy problem as a subset of all problems describable by our blended-objective cost function, we can guarantee that more solutions can be found

beyond the minimum-energy problem [1]. To do so, we formulated a control Lagrangian that blends the objectives of minimum-energy and minimum-fuel:

$$L = (1-\beta)\left\|u\right\|_2^2 + \beta\left\|u\right\|_2 \tag{28}$$

The associated control Hamiltonian is:

$$H = L + \lambda^T \mathbf{f} = (1-\beta)\left\|u\right\|_2^2 + \beta\left\|u\right\|_2 + \lambda^T \mathbf{f}_0 + +\lambda^T B\mathbf{u} \tag{29}$$

State and costate dynamics evolve as expected:

$$\dot{\mathbf{x}} = \mathbf{f}_0 + B\mathbf{u} \tag{30}$$

$$\dot{\lambda} = -A^T\lambda \tag{31}$$

And our optimal control is the control input $\mathbf{u}^*$ that satisfies:

$$\mathbf{u}^* = \underset{\left\|u\right\|_2 \leq u_{\max}}{\arg\min} \left((1-\beta)\left\|u\right\|_2^2 + \beta\left\|u\right\|_2 + \lambda^T B\mathbf{u}\right) \tag{32}$$

If we define the primer vector $\mathbf{p} = -B^T\lambda$ and substitute this in, we achieve:

$$\mathbf{u}^* = \underset{\left\|u\right\|_2 \leq u_{\max}}{\arg\min} \left((1-\beta)\left\|u\right\|_2^2 + \beta\left\|u\right\|_2 - \mathbf{p}^T\mathbf{u}\right) \tag{33}$$

We can decompose our control into $\mathbf{u} = \Gamma\hat{\mathbf{u}}$ and we note, regardless of the value of $\Gamma = \left\|\mathbf{u}\right\|_2$, $\hat{\mathbf{u}}$ has an optimal direction, $\hat{\mathbf{u}}^* = \hat{\mathbf{p}}$. Imposing this condition, we now have a one-parameter search for Γ^*

$$\Gamma^* = \underset{0\leq\Gamma\leq u_{\max}}{\arg\min} \left((1-\beta)\Gamma^2 + \beta\Gamma - \Gamma\left\|p\right\|_2 \hat{\mathbf{p}}^T\hat{\mathbf{p}}\right) \tag{34}$$

Or, simplifying and combining like terms:

$$\Gamma^* = \underset{0\leq\Gamma\leq u_{\max}}{\arg\min}\ (1-\beta)\Gamma^2 + (\beta - \left\|p\right\|_2)\Gamma \tag{35}$$

If $\beta \in (0,1)$ (noninclusive), the function we try to minimize is a concave-up parabola, $h(\Gamma)$. This function has a minimum at $\partial h/\partial\Gamma = 0$, or:

$$\frac{\partial\left[h(\Gamma)\right]}{\partial\Gamma} = 2(1-\beta)\Gamma + (\beta - \left\|p\right\|_2) = 0 \tag{36}$$

With $\Gamma_{\min}$:

$$\Gamma_{\min} = \frac{1}{2}\frac{\left\|p\right\|_2 - \beta}{1-\beta} \tag{37}$$

If $\Gamma_{\min}$ is greater than $u_{\max}$, then our thrust is limited by $u_{\max}$. In other words:

$$\frac{1}{2}\frac{\|p\|_2 - \beta}{1-\beta} > u_{\max} \Rightarrow \|p\|_2 - \beta > 2u_{\max}(1-\beta) \tag{38}$$

If $\Gamma_{\min}$ is less than 0, then our thrust should also be zero. In other words:

$$\frac{1}{2}\frac{\|p\|_2 - \beta}{1-\beta} < 0 \Rightarrow \|p\|_2 - \beta < 0 \tag{39}$$

And if $\Gamma_{\min}$ lies between 0 and $u_{\max}$, then it is our optimal thrust. Combining these into one piecewise function:

$$\Gamma^* = \begin{cases} u_{\max} & (2u_{\max}(1-\beta) < \|p\|_2 - \beta) \\ \frac{1}{2}\frac{\|p\|_2 - \beta}{1-\beta} & (0 \leq \|p\|_2 - \beta \leq 2u_{\max}(1-\beta)) \\ 0 & (\|p\|_2 - \beta < 0) \end{cases} \tag{40}$$

This function is defined in a piecewise fashion with two plateaus (one at zero, and one at $u_{\max}$) joined by a linear ramp. Generic ramp functions like this can be written as a combination of Heaviside step functions as follows:

$$f_{\text{ramp}}(x) = xH(x) - (x-1)H(x-1) \tag{41}$$

Which has the ramp beginning at $x = 0$, ending at $x = 1$ with plateaus at $f_{\text{ramp}}(x < 0) = 0$ and $f_{\text{ramp}}(x > 1) = 1$. For our use, the function needs to be scaled and shifted such that the ramp begins at $\|p\|_2 - \beta = 0$, ends at $\|p\|_2 - \beta = 2u_{\max}(1-\beta)$, with two plateaus at $f_{\text{ramp}}(\|p\|_2 - \beta < 0) = 0$ and $f_{\text{ramp}}(\|p\|_2 - \beta > 2u_{\max}(1-\beta)) = u_{\max}$. Furthermore, we can approximate the Heaviside step function $H(x)$ like:

$$H(x) \approx \frac{1}{2}\left[\frac{x}{\sqrt{x^2+\varepsilon^2}} + 1\right] \tag{42}$$

When $\varepsilon \ll 1$, the function strongly approximates the Heaviside step. When using this approximation and shifting/scaling the function as appropriate, we get a smooth approximant to our piecewise behavior:

$$\Gamma^*(\|p\|_2, \beta, \varepsilon) = \frac{1}{4(1-\beta)}\left[\frac{(\|p\|_2 - \beta)^2}{\sqrt{(\|p\|_2 - \beta)^2 + \varepsilon^2}} - \frac{(\|p\|_2 - \beta + 2u_{\max}(\beta-1))^2}{\sqrt{(\|p\|_2 - \beta + 2u_{\max}(\beta-1))^2 + \varepsilon^2}}\right] + \frac{u_{\max}}{2} \tag{43}$$

This smoothed function varies in four ways. The domain of the function is $\|p\|_2 \geq 0$, while we can parameterize the function with a choice of $\beta \in (0,1)$, $\varepsilon \ll 0$, and $u_{\max}$. By default, we will choose $\varepsilon = 0.01$ and $u_{\max}$ dependent on the specific homotopy we are hoping to achieve.

4 Results and Discussion

4.1 Minimum Energy

To initiate the minimum energy analysis, we defined a 48-hour window of catch opportunities. This window allows the payload multiple chances to successfully meet up with the tip of the tether, seperated by different values of Time-Of-Flight (TOF). First, a ballistic solution was found under uncontrolled dynamics that accomplished a successful rendezvous with the tether tip. The total 48-hour window surrounds this ballistic catch, 24-hours before and after. For the entire window, the payload was allowed to maneuver to accomplish catches throughout. The increments of time between trajectory samples within the catch window varies to counteract the dynamically-sensitive cislunar region. For this first analysis, the initial condition is fixed to better achieve smoother and consistent convergence.

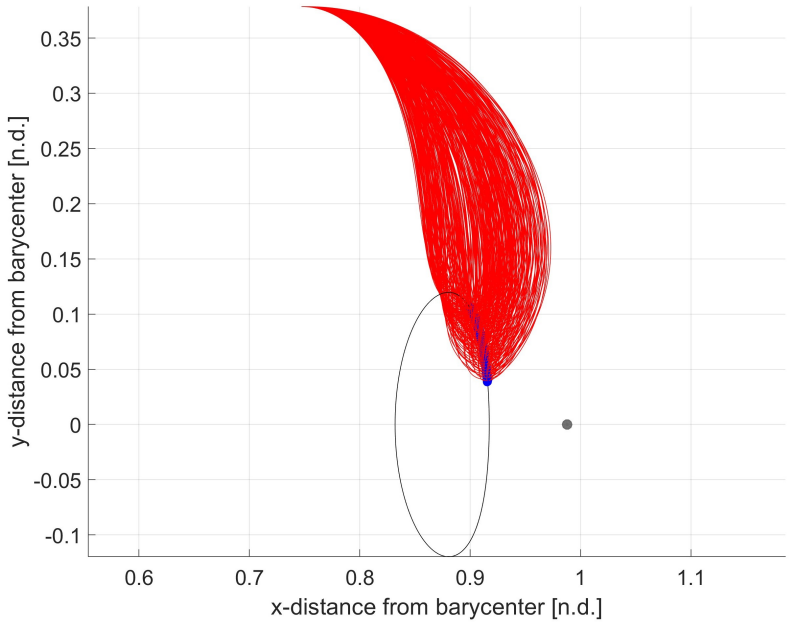

Figure 2: Trajectories of minimum energy solutions

Overall, minimum-energy controlled dynamics were simulated for the entire catch window ($N = 9792$ cases) and all cases successfully converged. Fig.2 shows a small sampling of the various TOF trajectories. As can be seen in the figure, different TOF options rendezvous with the tether in qualitatively different ways and at different locations due to the motion of the tether.

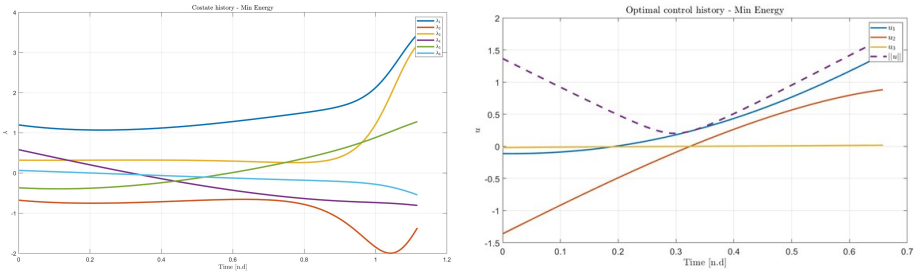

(a) Min. energy - costates history (b) Min. energy - optimal control history

Figure 3: Minimum energy results for one TOF

Fig.3 above shows a sample of the the costate and the optimal control history over time for just one TOF within the window. It is worth noting that optimal control should not go to zero towards the final time. Under minimum-energy dynamics, the payload could feasibly need to decelerate as it approaches the tether tip to successfully rendezvous.

4.2 Minimum Energy → Minimum Fuel Homotopy

In this part of the analysis, the same 48-hour catch window was analyzed to find minimum fuel solutions that corresponded to the already-converged minimum energy solutions. A shooting function was implemented to solve the Two Point Boundary Value Problem (TPBVP) for any β value used within the blended objective function as defined in Equation (28). Starting at $\beta = 0$ (which corresponds to a minimum energy problem) β was varied $\beta \in (0, 1)$ until $\beta = 1$ (where the problem becomes a minimum fuel objective function). The resulting converged conditions for each β value were fed into the next β process as an initial guess to achieve smoother convergence.

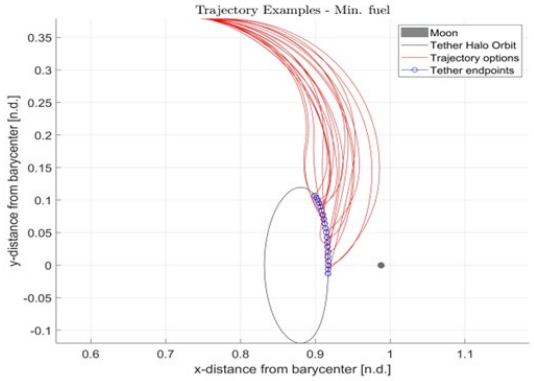

Figure 4: Sample trajectories from the homotopy ($\beta = 1$)

Figure 4 shows various sample trajectories from TOFs selected from the catch window.Visually apparent is that the trajectories for this case are quite different than the minimum-energy trajectories. Similar to the minimum energy case, a sample of the costate/optimal control histories for one TOF are plotted in Figure 5.

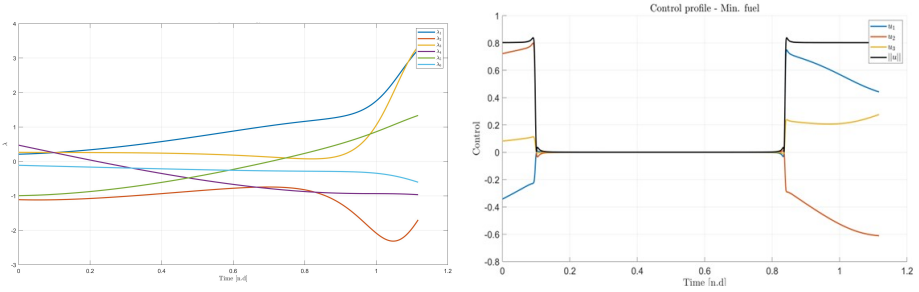

(a) Costates history ($\beta = 1$) (b) Bang-bang Control ($\beta = 1$)

Figure 5: Minimum fuel homotopy time histories for one TOF

As expected, the control profile is bang-bang. As a sanity check, we can use this behavior to justify that the homotopy resulted in feasible and locally-optimal results.

4.3 Aggregate Results

To futher validate the homotopy method, we can compare fuel costs between our sets of results. The fuel cost for both the minimum-energy and the minimum-fuel trajectory cases is computed and plotted.

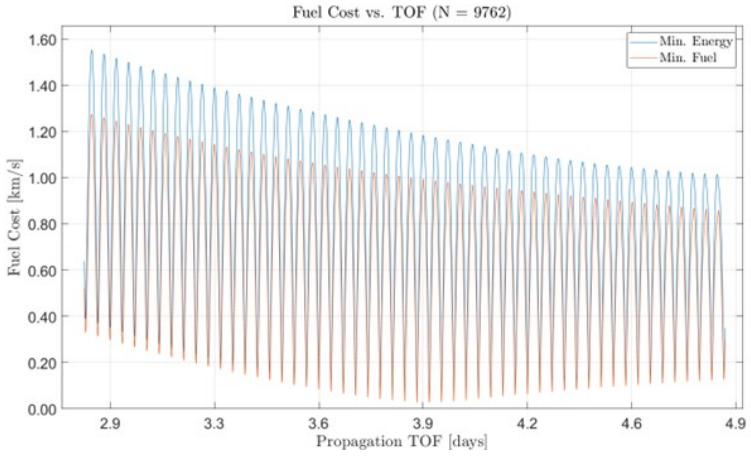

Figure 6: Comparison of Fuel cost vs TOF

Upon examining Figure 6, it is evident that the fuel cost for the minimum-fuel trajectories is indeed significantly lower than the fuel cost for the minimum energy trajectories. This result aligns with our expectations, as the minimum fuel homotopy solution is specifically optimized to minimize the fuel expenditure required for the payload to successfully rendezvous with the tether tip for all TOFs within the defined 48-hour catch window. This reduction in fuel cost can have far-reaching implications, such as extending the operational lifetime of the payload or enabling more ambitious mission objectives within the same fuel budget.

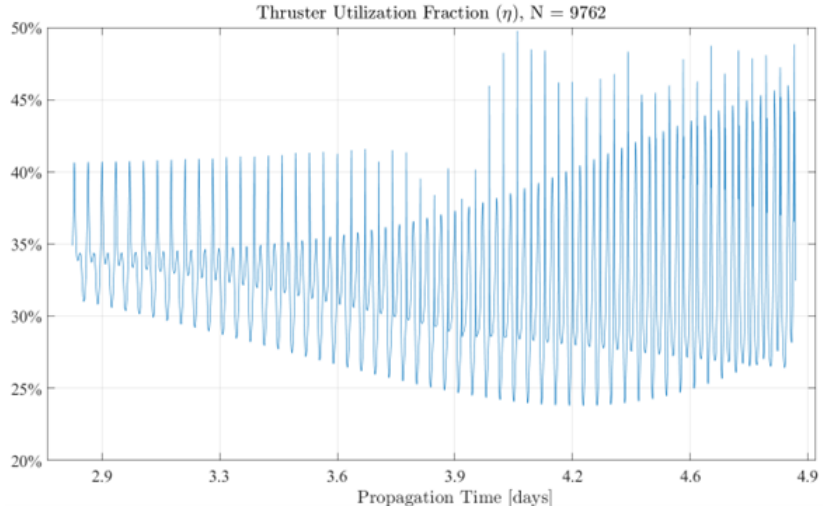

Figure 7: Thruster Utilization under minimum fuel homotopy

We can also plot other derived properties over the aggregate results. One interesting property worth visualizing is the *utilization fraction* of the thruster for each propogation. Over each propogation, we leverage the bang-bang nature of the control history to calculate this metric. For some portion of each integration, the thruster will be off and for some time it will be on. To do so, we measure what proportion of the time it is 'on' when compared against the total integration time. This number is calculated for each propogation, and is reported in Figure 7.

Measuring this utilization fraction can inform future analyses. For example on average over the entire catch window, the utilization fraction is only approximately $\eta = 35\%$, meaning that the thrusters are only used for about a third of the time. This number does vary considerably over the catch window (as small as $\eta = 25\%$ for some propogations, and as high as $\eta = 50\%$ for others). If for each propogation the thrust limit is changed, this utilization fraction will rise or fall accordingly. An interesting future direction of analysis could be using this metric to establish a *thrust limit floor*, or a measure of the weakest thruster

that can still achieve convergence. If the thruster has an original thrust maximum of $u^1_{\max}$, then to a first-order approximation, the weakest thruster that still achieves convergence will have a strength $u^2_{\max} = \eta_1 u^1_{\max}$. The true underlying relationship though is nonlinear, so the search for $u^{\min}_{\max}$ at a given TOF will require an iterative process.

5 Conclusions and Future Work

This study explored the optimal trajectory for a payload to successfully rendezvous with a tether stationed in a L_1 Halo orbit within the cislunar region. Under controlled dynamics, minimum energy solutions were derived for a 48-hour catch window. Additionally, for the same window, a continuation homotopy method was implemented to obtain a minimum fuel solution. One of the key insights from this project is that although the homotopy method works and provides locally optimal results, these results are not necessarily the ones desired. To elaborate, not all cases converged under the homotopy method, and even for converged cases, the solution did not guarantee alignment with the desired outcome. This limitation arises from the nature of the shooting function method, which finds locally optimal solutions but not globally optimal ones. One potential approach to mitigate such issues is to discretize the $\beta \in (0, 1)$ range into more samples, making the increment in values much smaller. Implementing this approach did help convergence, as the results of each converged β value are fed back as the initial guess for the next β value, thereby achieving better convergence. With tighter spacing between β values, this feedforward process yields initial guesses deeper within the convergence basin of future convergence processes.

All in all, the methods employed worked successfully for the given problem and the related objectives. By overcoming the challenges posed by highly sensitive dynamics, future studies may achieve more accurate and globally optimal minimum fuel solutions, thereby enhancing mission efficiency and enabling more ambitious space exploration endeavors in this dynamic region. While the CR3BP is a helpful model for modelling this region, more accurate dynamics could also be used. Future work could include maturing the dynamical model, perhaps into a high-fidelity ephemeris model.

The summary of each objective level is presented below:

5.1 Level 1: Minimum energy case

The procedure followed to arrive at the minimum energy solution for the payload to meet up with the tether tip provided satisfactory results. Equations shown in Section 3.1 are used to complete Level 1 of this project. A minimum energy solution for each TOFs within 48-hour catch opportunity was found. This approach provides minimum energy solutions that satisfy the terminal conditions

and we can confirm that they are indeed locally optimal (hence, a good) baseline for future Levels of this work.

5.2 Level 2: Minimum energy → Minimum fuel homotopy

For this objective, which corresponds to Level 2 of this project, a continuation homotopy method was used to achieve a smooth transition between the minimum energy and minimum fuel optimization problems. A shooting function was implemented in order to solve the homotopy method. Defining a sliding parameter, $\beta \in (0, 1)$ where the problem starts as a minimum energy problem when $\beta = 0$ and as a minimum fuel problem when $\beta = 1$. The converged conditions of each β is then fed back into the next β value as an initial guess to achieve a good smooth convergence. For each datapoint ($N = 9762$), this homotopy was accomplished using gradations in β of varying fineness. As promised by *Pontryagin's Minimum Principle*, this method does provide lower fuel costs when compared to a minimum-energy formulation. Analyzing results as an aggregate, it is also possible to theorize about a *minimum thrust floor*, something worth further analysis in future works

5.3 Level 3: Adding extensiblity to the tether

We did not complete the outlined Level 3 of this project. The derivations for how we would approach this level are provided in Section 6, but these derivations were not implemented successfully. Given the complex dynamics that would arise by adding an extensible tether, we did not have time to achieve this level.

However, if Level 3 would be accomplished, an extensible tether could potentially aid in total control efforts of the problem. This would lead to even less fuel expenditure increasing the efficiency and merit of using momentum exchange tethers to catch payloads. Perhaps also worthwhile, analyzing this Level using an alternate control scheme (*convex optimization*, for example) could yield similar results, at a much smaller implementation cost.

References

[1] Carl B. Allendoerfer. *Calculus of several variable and differentiable manifolds*. eng. New York: Macmillan, 1974. ISBN: 978-0-02-301840-4.

[2] Eugene L. Allgower and Kurt Georg. *Introduction to Numerical Continuation Methods*. en. Society for Industrial and Applied Mathematics, Jan. 2003. ISBN: 978-0-89871-544-6 978-0-89871-915-4. DOI: 10.1137/1.9780898719154. URL: http://epubs.siam.org/doi/book/10.1137/1.9780898719154 (visited on 05/29/2023).

[3] Yuki Kayama et al. "Low-Thrust Trajectory Design with Successive Convex Optimization for Libration Point Orbits". en. In: *Journal of Guidance, Control, and Dynamics* 45.4 (Apr. 2022), pp. 623–637. ISSN: 1533-3884. DOI: 10.2514/1.G005916. URL: https://arc.aiaa.org/doi/10.2514/1.G005916 (visited on 04/28/2024).

6 Appendices

6.1 A - Analytic Jacobian ODE Derivation

Analytic Jacobian for the CR3BP state/costate dynamics To provide the analytic derivative $\partial\Psi/\partial Z$ in general, we require some analytic work. For example, to use the analytic derivatives $\partial\mathbf{x}_f/\partial\lambda_0$, we must propogate the state-costate transition matrix (or the SCTM, for short). If we compose an augmented state:

$$\mathbf{X}_{aug} = \begin{bmatrix}\mathbf{x}\\ \lambda\end{bmatrix} \tag{44}$$

We can determine that the augmented state differential equations $\mathbf{F}(\mathbf{X}_{aug})$ are:

$$\mathbf{F}(\mathbf{X}_{aug}) = \begin{bmatrix}\mathbf{f}_0 + B\mathbf{u}\\ -A^T\lambda\end{bmatrix} = \begin{bmatrix}\mathbf{f}_0 - \frac{1}{2}BB^T\lambda\\ -A^T\lambda\end{bmatrix} \tag{45}$$

Where we've plugged in our optimal control for $\mathbf{u} = \mathbf{u}^*$

$$A = \frac{\partial\left[\mathbf{f}_0\right]}{\partial\mathbf{x}} = \begin{bmatrix}\mathbf{0}_{3\times3} & \mathbf{I}_{3\times3}\\ U_{pp} & \Omega\end{bmatrix} \tag{46}$$

In general, the state-costate transition matrix $\dot{\Phi}$ (truncated at linear terms) evolves according to the equation:

$$\dot{\Phi} = \left[\frac{\partial\left[\mathbf{F}\right]}{\partial\mathbf{X_{aug}}}\right]\Phi \tag{47}$$

$$\frac{\partial\left[\mathbf{F}\right]}{\partial\mathbf{X_{aug}}} = \begin{bmatrix}\frac{\partial}{\partial\mathbf{x}}\left[\mathbf{f}_0 - \frac{1}{2}BB^T\lambda\right] & \frac{\partial}{\partial\lambda}\left[\mathbf{f}_0 - \frac{1}{2}BB^T\lambda\right]\\ \frac{\partial}{\partial\mathbf{x}}\left[-A^T\lambda\right] & \frac{\partial}{\partial\lambda}\left[-A^T\lambda\right]\end{bmatrix} = \begin{bmatrix}A & -\frac{1}{2}BB^T\\ -\frac{\partial}{\partial\mathbf{x}}\left[A^T\lambda\right] & -A^T\end{bmatrix} \tag{48}$$

The only tricky derivative here is $-\frac{\partial}{\partial\mathbf{x}}\left[A^T\lambda\right]$, a derivative which, in it's full glory, produces a third-order tensor that is contracted back to a second-order tensor after post-multiplication by the costate. To avoid this mess, let's expand the tensor into it's constituent parts, maintaining coherence with our conventions for vector derivatives:

$$\begin{aligned}-\frac{\partial}{\partial\mathbf{x}}\left[A^T\lambda\right] &= -\begin{bmatrix}\left[\frac{\partial[A]}{\partial x}\right]^T\lambda & \left[\frac{\partial[A]}{\partial y}\right]^T\lambda & \left[\frac{\partial[A]}{\partial z}\right]^T\lambda & \left[\frac{\partial[A]}{\partial\dot{x}}\right]^T\lambda & \left[\frac{\partial[A]}{\partial\dot{y}}\right]^T\lambda & \left[\frac{\partial[A]}{\partial\dot{z}}\right]^T\lambda\end{bmatrix}\\ &= -\begin{bmatrix}\left[\frac{\partial[A]}{\partial x}\right]^T\lambda & \left[\frac{\partial[A]}{\partial y}\right]^T\lambda & \left[\frac{\partial[A]}{\partial z}\right]^T\lambda & \mathbf{0} & \mathbf{0} & \mathbf{0}\end{bmatrix}\end{aligned} \tag{49}$$

This row vector of column vectors contains four elements, each of which are easy to compute using our standard matrix calculus rules. We can now work to get

a good definition of the matrix $\left[\frac{\partial[A]}{\partial x}\right]^T$, the partial derivative of a matrix with respect to a scalar:

$$\left[\frac{\partial\,[A]}{\partial x}\right]^T = \begin{bmatrix} \mathbf{0}_{3\times3} & \frac{\partial}{\partial x}\,[U_{pp}] \\ \mathbf{0}_{3\times3} & \mathbf{0}_{3\times3} \end{bmatrix} \tag{50}$$

Note that the derivatives $\left[\frac{\partial}{\partial y}\,[A]\right]^T$ and $\left[\frac{\partial}{\partial z}\,[A]\right]^T$ (also needed) will have very similar forms. Sparing the gory details (available upon request), $\frac{\partial[U_{pp}]}{\partial x}$, $\frac{\partial[U_{pp}]}{\partial y}$ and $\frac{\partial[U_{pp}]}{\partial z}$ have analytic derivatives. U_{pp} is a symmetric matrix:

$$U_{pp} = \begin{bmatrix} \frac{\partial}{\partial x\partial x}\,[U] & \frac{\partial}{\partial x\partial y}\,[U] & \frac{\partial}{\partial x\partial z}\,[U] \\ \frac{\partial}{\partial y\partial x}\,[U] & \frac{\partial}{\partial y\partial y}\,[U] & \frac{\partial}{\partial y\partial z}\,[U] \\ \frac{\partial}{\partial z\partial x}\,[U] & \frac{\partial}{\partial z\partial y}\,[U] & \frac{\partial}{\partial z\partial z}\,[U] \end{bmatrix} = \begin{bmatrix} \frac{\partial}{\partial x\partial x}\,[U] & \frac{\partial}{\partial x\partial y}\,[U] & \frac{\partial}{\partial x\partial z}\,[U] \\ - & \frac{\partial}{\partial y\partial y}\,[U] & \frac{\partial}{\partial y\partial z}\,[U] \\ - & - & \frac{\partial}{\partial z\partial z}\,[U] \end{bmatrix} \tag{51}$$

And the various symmetric partial derivative matrices are:

$$\frac{\partial\,[U_{pp}]}{\partial x} = \begin{bmatrix} \frac{\partial}{\partial x\partial x\partial x}\,[U] & \frac{\partial}{\partial x\partial y\partial x}\,[U] & \frac{\partial}{\partial x\partial z\partial x}\,[U] \\ \frac{\partial}{\partial y\partial x\partial x}\,[U] & \frac{\partial}{\partial y\partial y\partial x}\,[U] & \frac{\partial}{\partial y\partial z\partial x}\,[U] \\ \frac{\partial}{\partial z\partial x\partial x}\,[U] & \frac{\partial}{\partial z\partial y\partial x}\,[U] & \frac{\partial}{\partial z\partial z\partial x}\,[U] \end{bmatrix} = \begin{bmatrix} U_{xxx} & U_{xxy} & U_{xxz} \\ - & U_{xyy} & U_{xyz} \\ - & - & U_{xzz} \end{bmatrix} \tag{52}$$

$$\frac{\partial\,[U_{pp}]}{\partial y} = \begin{bmatrix} \frac{\partial}{\partial x\partial x\partial y}\,[U] & \frac{\partial}{\partial x\partial y\partial y}\,[U] & \frac{\partial}{\partial x\partial z\partial y}\,[U] \\ \frac{\partial}{\partial y\partial x\partial y}\,[U] & \frac{\partial}{\partial y\partial y\partial y}\,[U] & \frac{\partial}{\partial y\partial z\partial y}\,[U] \\ \frac{\partial}{\partial z\partial x\partial y}\,[U] & \frac{\partial}{\partial z\partial y\partial y}\,[U] & \frac{\partial}{\partial z\partial z\partial y}\,[U] \end{bmatrix} = \begin{bmatrix} U_{xxy} & U_{xyy} & U_{xyz} \\ - & U_{yyy} & U_{yyz} \\ - & - & U_{yzz} \end{bmatrix} \tag{53}$$

$$\frac{\partial\,[U_{pp}]}{\partial z} = \begin{bmatrix} \frac{\partial}{\partial x\partial x\partial z}\,[U] & \frac{\partial}{\partial x\partial y\partial z}\,[U] & \frac{\partial}{\partial x\partial z\partial z}\,[U] \\ \frac{\partial}{\partial y\partial x\partial z}\,[U] & \frac{\partial}{\partial y\partial y\partial z}\,[U] & \frac{\partial}{\partial y\partial z\partial z}\,[U] \\ \frac{\partial}{\partial z\partial x\partial z}\,[U] & \frac{\partial}{\partial z\partial y\partial z}\,[U] & \frac{\partial}{\partial z\partial z\partial z}\,[U] \end{bmatrix} = \begin{bmatrix} U_{xxz} & U_{xyz} & Uxzz \\ - & U_{yyz} & U_{yzz} \\ - & - & U_{zzz} \end{bmatrix} \tag{54}$$

While eighteen derivatives are present in the equations above, only ten are unique. The matrices have the following structure:

$$\frac{\partial\,[U_{pp}]}{\partial x} = \begin{bmatrix} [1] & [2] & [3] \\ - & [4] & [5] \\ - & - & [6] \end{bmatrix} \quad \frac{\partial\,[U_{pp}]}{\partial y} = \begin{bmatrix} [2] & [4] & [5] \\ - & [7] & [8] \\ - & - & [9] \end{bmatrix} \quad \frac{\partial\,[U_{pp}]}{\partial z} = \begin{bmatrix} [3] & [5] & [6] \\ - & [8] & [9] \\ - & - & [10] \end{bmatrix} \tag{55}$$

Where the ten unique derivatives are:

The final form of $-\frac{\partial}{\partial \mathbf{x}}\left[A^T\lambda\right]$ (required for our state-costate transition matrix)

Positional element	Corresponding derivative
[1]	U_{xxx}
[2]	U_{xxy}
[3]	U_{xxz}
[4]	U_{xyy}
[5]	U_{xyz}
[6]	U_{xzz}
[7]	U_{xyy}
[8]	U_{yyz}
[9]	U_{yzz}
[10]	U_{zzz}

is the 6×6 matrix. Let's call $M = -\frac{\partial}{\partial \mathbf{x}}\left[A^T\lambda\right]$:

$$\begin{aligned} M = -\frac{\partial}{\partial \mathbf{x}}\left[A^T\lambda\right] &= -\begin{bmatrix} \left[\frac{\partial [A]}{\partial x}\right]^T\lambda & \left[\frac{\partial [A]}{\partial y}\right]^T\lambda & \left[\frac{\partial [A]}{\partial z}\right]^T\lambda & \mathbf{0} & \mathbf{0} & \mathbf{0} \end{bmatrix} \\ &= -\begin{bmatrix} \frac{\partial}{\partial x}\left[U_{pp}\right]\lambda_{4-6} & \frac{\partial}{\partial y}\left[U_{pp}\right]\lambda_{4-6} & \frac{\partial}{\partial z}\left[U_{pp}\right]\lambda_{4-6} & \mathbf{0} & \mathbf{0} & \mathbf{0} \\ \mathbf{0} & \mathbf{0} & \mathbf{0} & \mathbf{0} & \mathbf{0} & \mathbf{0} \end{bmatrix} \end{aligned} \tag{56}$$

Where λ_{4-6} is a column vector containing the last three elements of the costate, and all zero vectors are $\mathbf{0} = \begin{bmatrix} 0, & 0, & 0 \end{bmatrix}^T$. With some algebraic simplification, the matrix governing the evolution of our state-costate transition matrix is the structured block matrix:

$$\frac{\partial\left[\mathbf{F}\right]}{\partial \mathbf{X_{aug}}} = \begin{bmatrix} \begin{bmatrix} \mathbf{0}_{3\times3} & \mathbf{I}_{3\times3} \\ U_{pp} & \Omega \end{bmatrix} & \begin{bmatrix} \mathbf{0}_{3\times3} & \mathbf{0}_{3\times3} \\ \mathbf{0}_{3\times3} & -\frac{1}{2}I_{3\times3} \end{bmatrix} \\ M & \begin{bmatrix} \mathbf{0}_{3\times3} & -U_{pp} \\ -\mathbf{I}_{3\times3} & -\Omega \end{bmatrix} \end{bmatrix} \tag{57}$$

Since U_{pp} and the identity matrix are symmetric. Note that only U_{pp} and M change over the trajectory, while all other block matrices are constant.

6.2 B - Level 3: Extensible tether (INCOMPLETE)

Author's note: We think that PMP is the wrong path to follow for this section. It seems much more likely that this will succeed if convex optimization is used instead.

Let's define the tether's current angle to be α with respect to an inertial frame, its angular velocity to be $\dot{\alpha}$, and its angular acceleration to be $\ddot{\alpha}$. Let's define the relative angle between the tether and the synodic frame $\beta = n(t-t_0) - \alpha$. We'd like to add an ability to the tether to extend and contract. By the conservation of angular momentum, the tether should then spin faster or slower. Theoretically,

this change in spin rate predicates more favorable encounters and less fuel cost required of the payloads. The angular momentum of the tether $\mathbf{H} = I\dot{\alpha}$ is a constant. If we model the tether as a thin cylinder rotating about it's endpoint, the tether has a moment of inertia of $\rho L^3/3$, where M is the total mass of the tether, L is it's length and ρ is a linear density. Making a substitution for the moment of inertia and taking the time derivative of the angular momentum:

$$\frac{d}{dt}\left[\frac{\rho}{3}L^3\dot{\alpha}\right] = \frac{\rho}{3}\left[3L^2\dot{L}\dot{\alpha} + L^3\ddot{\alpha}\right] = 0 \tag{58}$$

If we solve for $\ddot{\alpha}$, we can get a simple control law for it in terms of $\dot{L}$:

$$-\frac{3\dot{\alpha}\dot{L}}{L} = \ddot{\alpha} \tag{59}$$

We can define a direct rotation from the tether's body frame into the Earth-Moon synodic frame as follows

$$C_{\mathcal{B}\to\mathcal{S}} = \begin{bmatrix} \cos\beta & \sin\beta & 0 \\ -\sin\beta & \cos\beta & 0 \\ 0 & 0 & 1 \end{bmatrix} \tag{60}$$

The time derivative of this matrix is:

$$\dot{C}_{\mathcal{B}\to\mathcal{S}} = \frac{d\beta}{dt}\begin{bmatrix} -\sin\beta & \cos\beta & 0 \\ -\cos\beta & -\sin\beta & 0 \\ 0 & 0 & 0 \end{bmatrix} = (n-\dot{\alpha})\begin{bmatrix} -\sin\beta & \cos\beta & 0 \\ -\cos\beta & -\sin\beta & 0 \\ 0 & 0 & 0 \end{bmatrix} \tag{61}$$

Or, more simply, $\dot{C}_{\mathcal{B}\to\mathcal{S}} = (n-\dot{\alpha})\tilde{C}$ and the second time derivative is:

$$\ddot{C}_{\mathcal{B}\to\mathcal{S}} = -\ddot{\alpha}\tilde{C} - (n-\dot{\alpha})^2 C_{\mathcal{B}\to\mathcal{S}} \tag{62}$$

We can define the motion of the tip of the tether as we've done before:

$$\mathbf{h}_{\text{tip}} = \mathbf{r}_{\text{halo}} + \mathbf{r}_{\text{delta}} \tag{63}$$

And recognize that vectors between two rotating frames transform like:

$$\begin{bmatrix} {}^{\mathcal{S}}\vec{x} \\ {}^{\mathcal{S}}\dot{\vec{x}} \\ {}^{\mathcal{S}}\ddot{\vec{x}} \end{bmatrix} = \begin{bmatrix} C_{\mathcal{B}\to\mathcal{S}} & 0 & 0 \\ \dot{C}_{\mathcal{B}\to\mathcal{S}} & C_{\mathcal{B}\to\mathcal{S}} & 0 \\ \ddot{C}_{\mathcal{B}\to\mathcal{S}} & 2\,\dot{C}_{\mathcal{B}\to\mathcal{S}} & C_{\mathcal{B}\to\mathcal{S}} \end{bmatrix} \begin{bmatrix} {}^{\mathcal{B}}\vec{x} \\ {}^{\mathcal{B}}\dot{\vec{x}} \\ {}^{\mathcal{B}}\ddot{\vec{x}} \end{bmatrix} \tag{64}$$

The vector we wish to transform is a stationary point within frame $\mathcal{B}$ is just comprised of a positional component in the $\mathcal{B}$-frame's first direction, a vector equal

to $\begin{bmatrix} L, & 0, & 0, & 0, & 0, & 0, & 0, & 0, & 0 \end{bmatrix}^T$. Simplifying, we can write the synodic frame representation of this vector, the corresponding velocity and acceleration:

$$\begin{aligned} {}^{\mathcal{S}}\mathbf{r}_{\text{delta}} &= C_{\mathcal{B}\to\mathcal{S}}\,{}^{\mathcal{B}}\mathbf{r}_{\text{delta}} \\ {}^{\mathcal{S}}\dot{\mathbf{r}}_{\text{delta}} &= \dot{C}_{\mathcal{B}\to\mathcal{S}}\,{}^{\mathcal{B}}\mathbf{r}_{\text{delta}} = (n-\dot{\alpha})\tilde{C}\ {}^{\mathcal{B}}\mathbf{r}_{\text{delta}} \\ {}^{\mathcal{S}}\ddot{\mathbf{r}}_{\text{delta}} &= \ddot{C}_{\mathcal{B}\to\mathcal{S}}\,{}^{\mathcal{B}}\mathbf{r}_{\text{delta}} = -(\ddot{\alpha}\tilde{C} + (n-\dot{\alpha})^2 C_{\mathcal{B}\to\mathcal{S}})\ {}^{\mathcal{B}}\mathbf{r}_{\text{delta}} \end{aligned} \tag{65}$$

By adding these quantities to the tether center of mass's motion in the synodic frame, we can achieve a proper synodic representation of the tip of the tether's motion. If we wish to make the tether extensible, we require an augmented state vector, dynamics, control and B vector. Very concisely (and in nondimensional form:

$$\vec{x} = \begin{bmatrix} x \\ y \\ z \\ \dot{x} \\ \dot{y} \\ \dot{z} \\ l \\ \alpha \\ \dot{\alpha} \end{bmatrix} \qquad \mathbf{f}_0(\mathbf{x},t) = \begin{bmatrix} \dot{\mathbf{x}} \\ \dot{\mathbf{y}} \\ \dot{\mathbf{z}} \\ f_x \\ f_y \\ f_z \\ 0 \\ \dot{\alpha} \\ 0 \end{bmatrix} \qquad \vec{u} = \begin{bmatrix} u_x \\ u_y \\ u_z \\ \dot{l} \end{bmatrix} \qquad B = \begin{bmatrix} 0 & 0 & 0 & 0 \\ 0 & 0 & 0 & 0 \\ 0 & 0 & 0 & 0 \\ 1 & 0 & 0 & 0 \\ 0 & 1 & 0 & 0 \\ 0 & 0 & 1 & 0 \\ 0 & 0 & 0 & 1 \\ 0 & 0 & 0 & 0 \\ 0 & 0 & 0 & \gamma \end{bmatrix} \tag{66}$$

Where $\gamma = -3\dot{\alpha}/l$. We can formulate a control Lagrangian to penalize only thruster burns, under the assumption that tether adjustments are 'free' by comparison:

$$\mathcal{L} = \delta \left\|\mathbf{u}_T\right\|_2 + \dot{l}^2(1-\delta) \tag{67}$$

where the control subvector $\mathbf{u}_T = \begin{bmatrix} u_x, & u_y, & u_z \end{bmatrix}^T$. Our control Hamiltonian becomes:

$$H = L + \lambda^T(\mathbf{f}_0 + B\mathbf{u}) \tag{68}$$

Our state evolves as expected, while our costate evolves like:

$$\dot{\lambda}^T = -H_{\mathbf{x}} = -\lambda^T \frac{\partial}{\partial \mathbf{x}}\left[\mathbf{f}_0 + B\mathbf{u}\right] = -\lambda^T \frac{\partial\left[\mathbf{f}_0\right]}{\partial \mathbf{x}} - \lambda^T \frac{\partial\left[B\mathbf{u}\right]}{\partial \mathbf{x}} \tag{69}$$

$$\frac{\partial\left[\mathbf{f}_0\right]}{\partial \mathbf{x}} = \begin{bmatrix} A & & \mathbf{0}_{6\times 3} \\ & 0 & 0 & 0 \\ \mathbf{0}_{3\times 6} & 0 & 0 & 1 \\ & 0 & 0 & 0 \end{bmatrix} \tag{70}$$

$$\frac{\partial\left[B\mathbf{u}\right]}{\partial \mathbf{x}} = \begin{bmatrix} 0, & 0, & 0, & 0, & 0, & 0, & \frac{\partial[B]}{\partial l}\mathbf{u}, & 0, & \frac{\partial[B]}{\partial \dot{\alpha}}\mathbf{u} \end{bmatrix} \tag{71}$$

For this equation, we hypothetically need our optimal contraction rate $\dot{l}^*$ which we'll solve for later. Until then, $\frac{\partial[B]}{\partial l}\mathbf{u} = \begin{bmatrix} 0, & 0, & 0, & 0, & 0, & 0, & 0, & 0, & \frac{\partial[\gamma]}{\partial l}\dot{l}^* \end{bmatrix}^T$ and $\frac{\partial[B]}{\partial \dot{\alpha}}\mathbf{u} = \begin{bmatrix} 0, & 0, & 0, & 0, & 0, & 0, & 0, & 0, & \frac{\partial[\gamma]}{\partial \dot{\alpha}}\dot{l}^* \end{bmatrix}^T$.

$$\frac{\partial\left[\gamma\right]}{\partial l} = 3\dot{\alpha}/l^2 \qquad\qquad \frac{\partial\left[\gamma\right]}{\partial \dot{\alpha}} = -3/l \tag{72}$$

If we add the two 9×9 matrices, we can define a new matrix G:

$$G = \frac{\partial\left[\mathbf{f}_0\right]}{\partial \mathbf{x}} + \frac{\partial\left[B\mathbf{u}\right]}{\partial \mathbf{x}} = \begin{bmatrix} A & & \mathbf{0}_{6\times 3} & \\ & 0 & 0 & 0 \\ \mathbf{0}_{3\times 6} & 0 & 0 & 1 \\ & 3\dot{\alpha}\dot{l}^*/l^2 & 0 & -3\dot{l}^*/l \end{bmatrix} \tag{73}$$

And the costate evolves according to:

$$\boxed{\dot{\lambda} = -G^T\lambda} \tag{74}$$

Our optimal control is the control input $\{\mathbf{u}_T^*,\ \dot{l}^*\}$ that satisfies:

$$\begin{aligned} \{\mathbf{u}_T^*,\ \dot{l}^*\} &= \underset{\|\mathbf{u}_T\|_2 \le u_{\max},\ \|\dot{l}\|_2 \le \dot{l}_{\max}}{\arg\min} \quad \delta\left\|\mathbf{u}_T\right\|_2 + \dot{l}^2(1-\delta) + \lambda^T(\mathbf{f}_0 + B\mathbf{u}) \\ &= \underset{\|\mathbf{u}_T\|_2 \le u_{\max},\ \|\dot{l}\|_2 \le \dot{l}_{\max}}{\arg\min} \quad \delta\left\|\mathbf{u}_T\right\|_2 + \dot{l}^2(1-\delta) + \lambda^T B\mathbf{u} \end{aligned} \tag{75}$$

If we define $\tilde{\lambda}$ to be the first six elements of λ, we can further decompose our control Hamiltonian:

$$\{\mathbf{u}_T^*,\ \dot{l}^*\} = \underset{\|\mathbf{u}_T\|_2 \le u_{\max},\ \|\dot{l}\|_2 \le \dot{l}_{\max}}{\arg\min} \quad \delta\left\|\mathbf{u}_T\right\|_2 + \dot{l}^2(1-\delta) + \tilde{\lambda}^T\tilde{B}\mathbf{u}_T + \dot{l}\left(\lambda_7 + \gamma\lambda_9\right) \tag{76}$$

We can decompose $\mathbf{u}_T = \Gamma\hat{\mathbf{u}}$ and define a primer vector $\tilde{p} = -\tilde{B}^T\tilde{\lambda}$. Noting that the Hamiltonian is minimized when this primer vector and $\mathbf{u}_T$ are colinear, we can surmise that $\hat{u}^* = \hat{p}$:

$$\begin{aligned} \{\Gamma^*,\ \dot{l}^*\} &= \underset{\Gamma \le u_{\max},\ \|\dot{l}\|_2 \le \dot{l}_{\max}}{\arg\min} \quad \delta\cdot\Gamma - \Gamma\left\|\tilde{p}\right\|_2\ (\hat{\mathbf{p}}^T\hat{\mathbf{p}}) + \dot{l}^2(1-\delta) + \dot{l}\left(\lambda_7 + \gamma\lambda_9\right) \\ &= \underset{\Gamma \le u_{\max},\ \|\dot{l}\|_2 \le \dot{l}_{\max}}{\arg\min} \quad \Gamma(\delta - \left\|\tilde{p}\right\|_2) + \dot{l}^2(1-\delta) + \dot{l}\left(\lambda_7 + \gamma\lambda_9\right) \end{aligned} \tag{77}$$

With some analysis of the expression, we can see that the terms for Γ and the terms for $\dot{l}$ are mutually exclusive - if each is minimized separately, then their combination will also be minimized. This leads to the definition of Γ^*:

$$\Gamma^* = \begin{cases} u_{\max} & (\|\tilde{p}\|_2 \geq \delta) \\ 0 & (\|\tilde{p}\|_2 < \delta) \end{cases} \tag{78}$$

The terms of $\dot{l}^*$ are a quadratic form. The minimum of this quadratic expression is at the point:

$$\dot{l}_{\min} = \frac{1}{2} \frac{\lambda_7 + \gamma\lambda_9}{\delta - 1} \tag{79}$$

And, like our analysis before, we need to compare this against our bounds for $\dot{l}$. Doing this again, we get a piecewise representation of $\dot{l}^*$. If we define $s = \lambda_7 + \gamma\lambda_9$ and $\tilde{s} = 2(\delta - 1)\dot{l}_{\max}$:

$$\dot{l}^* = \begin{cases} -\dot{l}_{\max} & (s < -\tilde{s}) \\ +\dot{l}_{\max} & (s > +\tilde{s}) \\ \frac{s}{2}\frac{1}{\delta - 1} & (-\tilde{s} \leq s \leq \tilde{s}) \end{cases} \tag{80}$$

Both of these switching functions can be defined analytically using the Heaviside step function $\mathcal{H}(x)$.

$$\begin{aligned} \Gamma^* &= u_{\max}\, \mathcal{H}(\|\tilde{p}\|_2 - \delta) \\ \dot{l}^* &= \frac{\dot{l}_{\max}}{\tilde{s}} \Big[(s + \tilde{s})\mathcal{H}(s + \tilde{s}) - (s - \tilde{s})\mathcal{H}(s - \tilde{s}) \Big] - \dot{l}_{\max} \end{aligned} \tag{81}$$

Using the same approximation as earlier:

$$\Gamma^* = u_{\max}\, \mathcal{H}(\|\tilde{p}\|_2 - 1) \approx \frac{u_{\max}}{2} \left[\frac{\|(\tilde{p}\|_2 - 1)}{\sqrt{(\|\tilde{p}\|_2 - 1)^2 + \kappa_u^2}} + 1 \right] \tag{82}$$

$$\dot{l}^* \approx \frac{\dot{l}_{\max}}{2\,\tilde{s}} \left[\frac{(s + \tilde{s})^2}{\sqrt{(s + \tilde{s})^2 + \kappa_l^2}} - \frac{(s - \tilde{s})^2}{\sqrt{(s - \tilde{s})^2 + \kappa_l^2}} \right] - \dot{l}_{\max} \tag{83}$$